Materials Today Energy 21 (2021) 100750

Contents lists available at ScienceDirect

Materials Today Energy

journal homepage: www.journals.elsevier.com/materials-today-energy/

Understanding impacts of flow rate on performance of desalination flow batteries

F. Wang [a, d], W. Wu [a, d], Z. Lu [a, b], B. Yuan [b], Y. Zhao [c, **], T.L. Liu [a, *]

[a] Department of Chemistry and Biochemistry, Utah State University, Logan, UT, 84322, USA
[b] State Key Laboratory Base of Eco-chemical Engineering, College of Chemistry and Molecular Engineering, Qingdao University of Science and Technology, Qingdao, 266042, China
[c] Key Laboratory of Marine Chemistry Theory and Technology, Ministry of Education, College of Chemistry and Chemical Engineering, Ocean University of China, Qingdao, 266100, China

ARTICLE INFO

Article history:
Received 10 February 2021
Received in revised form
16 March 2021
Accepted 5 April 2021
Available online 15 April 2021

Keywords:
Energy storage
Freshwater
Flow battery
Ferrocyanide
Viologen

ABSTRACT

It is critical to develop more efficient and cost-effective desalination technologies capable of fully seawater desalination capacity to meet the grand freshwater scarcity challenge. Desalination flow batteries are an emerging electrochemical device capable of integrated energy storage and desalination and represent a promising electrochemical technology for scalable and cost-effective desalination of seawater. Herein, we report the impacts of flow rate on the performance of a methyl viologen/sodium ferrocyanide ($MV/Na_4[Fe(CN)_6]$) desalination flow battery (DSRFB). It was found that the increase of the flow rate can lower the battery resistance and improve energy efficiencies, power density, and desalination efficiency. Specifically, increasing the flow rate from 20 to 60 mL/min with an increment of 20 mL/min, the $MV/Na_4[Fe(CN)_6]$ DSRFB manifested an increase of energy efficiency from 56% to 64%, and an increase of power density from 14.72 to 15.33 mW/cm^2. More importantly, the desalination percentage of the DSRFB was increased from 86.9% at 20 mL/min to 93.9% at 60 mL/min.

1. Introduction

Freshwater scarcity is regarded as a global grand challenge faced by the development of modern society [1–3]. The increasing consumption of fresh water is essentially driven by the continuous growth of global human population [1]. It is of no doubt that we need to develop new recourses of fresh water. Oceans occupy 97% of the total water of the planet and thus represents the most abundant and sustainable water resource. However, seawater's high salinity (ca. 0.56 M of NaCl as simulation) must first be removed to meet the needs of human consumption, agriculture, and other purposes. Reverse osmosis represents a widely adopted commercial desalination technique of seawater, but its high costs (>$0.53/$m^3$) and high energy consumption (ca. > 3 Wh/L water production) to produce fresh water are the limiting factors for widespread implementation [1,4]. Efforts have been made to develop electrochemical desalination technologies including electrodialysis, capacitive deionization, and faradaic deionization that have offered alternative means for saltwater desalination [5]. However, solid-state electrodes including capacitive and faradic electrodes used in these systems are a limiting factor for desalination capacities of these desalination devices and most has been demonstrated for the desalination of low salinity (typically less than 0.1 M) [5]. Thus, it is critical to develop more efficient and cost-effective electrochemical desalination technologies capable of fully seawater desalination capacity while enabling the use of renewable electricity from solar and wind.

Aqueous organic redox flow batteries (AORFBs) using structurally tunable redox active organic and organometallic molecules have received increasingly attention for high performance, affordable, sustainable large-scale energy storage [6–9]. AORFBs using water-soluble, structurally tunable, redox active molecules including viologen (anolyte) [10–17], quinone (anolyte) [18–20], phenazine (anolyte) [21], TEMPO (catholyte) [10,14,15], ferrocene (catholyte) [11,16], ferrocyanide (catholyte) [22–24], and phenothiazine (catholyte) [25] have been extensively demonstrated with outstanding energy storage performance. Particularly, pH neutral

* Corresponding author.
** Corresponding author.
E-mail addresses: rain@ouc.edu.cn (Y. Zhao), leo.liu@usu.edu, liugrouppub@gmail.com (T.L. Liu).
[d] Equal contributions to this work.

https://doi.org/10.1016/j.mtener.2021.100750
2468-6069/

AORFBs with their stable cycling performance and non-corrosive nature are readily adapted for coupled energy storage and desalination functions [10–14,16,22,26]. Recently we and others have developed desalination flow batteries with integrated desalination and energy storage dual functions [27–30]. Fig. 1 illustrates the general design of the emerging three-channel dual membrane desalination flow batteries using a methyl viologen anolyte and a $Na_4[Fe(CN)_6]$ catholyte reported by us [30]. Compared with the traditional two-channel one membrane flow batteries, the desalination flow batteries incorporate an additional central channel and an additional membrane for salination and desalination of seawater during battery operation.

Herein, we use the MV/$Na_4[Fe(CN)_6]$ desalination flow battery (where MV is dimethyl viologen dichloride) recently reported by us to explain the working principle of a desalination flow battery (DSRFB, Fig. 1) [30]. During the charge process, MV is reduced to give off an equivalent of Cl^- anions, whereas $Na_4[Fe(CN)_6]$ is oxidized to release an equivalent of Na^+ cations. The Cl^- anion and the Na^+ cation will be combined in the central channel by migrating through an anion exchange membrane and a cation exchange membrane, respectively. Before discharge, the central channel will be replaced with a new batch of salt water. Then, the Cl^- and Na^+ ions will transport from the central channel to the MV anolyte and $Na_4[Fe(CN)_6]$ catholyte during discharge process to balance charge neutrality and achieve the desalination for the salt water in the central channel. The cell redox reactions of the MV anolyte and $Na_4[Fe(CN)_6]$ catholyte are provided in Fig. 1. Desalination flow batteries reserve the technological merits of traditional flow batteries for coupled desalination and energy storage, including decoupled energy and power operation, high current and high power performance, scalability, and safety features. This MV/$Na_4[Fe(CN)_6]$ DSRFB was able to desalinate simulated seawater (0.56 M NaCl) and Pacific Ocean water more than 98.5% at a rate of 4.55 mL of fresh water per hour and an energy cost of 2.4 Wh/L of fresh water—competitive with current reverse osmosis technologies [30]. Simultaneously, the cell delivered stored energy at 76.7% efficiency with a cell voltage of 0.91 V. This MV/$Na_4[Fe(CN)_6]$ DSRFB stands for the state of the art desalination flow battery to date [30]. In addition, methyl viologen has been applied in a four-channel flow battery for solo desalination function, but this system has no energy storage capability [31]. $Na_4[Fe(CN)_6]$ was used as a catholyte in a Zn/$Na_4[Fe(CN)_6]$ DSRFB. However, simple metal $ZnCl_2$ salt used as an anolyte is prone to crossover and causes irreversible capacity loss, thus reducing the cycling life of the DSRFB. Moreover, the Zn system using the solid $Zn^{2+/0}$ redox chemistry loses the merit of the decoupled energy and power of standard all-flow RFBs [27]. In this communication, we present a study to understand how flow dynamics influences the desalination and energy storage performance of the MV/$Na_4[Fe(CN)_6]$ DSRFB. We found that the increase of flow rate can increase the mass transfer speed and reduce the ohmic and charge transfer resistances of the battery to simultaneously improve desalination efficiency, energy efficiency, and power performance. The present results are expected to be highly valuable to develop optimal operation conditions for future desalination flow batteries.

2. Results and discussion

2.1. Energy storage and desalination performance of the $MVCl_2$/$Na_4[Fe(CN)_6]$ DSRFB at different flow rates

The MV/$Na_4[Fe(CN)_6]$ desalination DSRFB was built by using 0.5 M dimethyl viologen dichloride (MV, −0.45 V vs. NHE) as an anolyte material and 0.5 M $Na_4[Fe(CN)_6]$ (+0.46 V vs. NHE) as a catholyte material in accordance with our previous publication [30]. NaCl (2.0 M) was added as the supporting electrolyte in the anolyte side to reach a high conductivity (170.2 mS/cm). No extra salt was used in the catholyte side because of high ion strength and high conductivity (123.3 mS/cm) of $Na_4[Fe(CN)_6]$. The pH values of the anolyte and catholyte were adjusted to 7 using NaOH and HCl, respectively. Specifically, the DSRFB was demonstrated by using 15 mL anolyte, 15 mL catholyte, and 10 mL of simulated sea water (0.56 M NaCl) in the central chamber (see Fig. 1). A piece of Selemion AMV membrane was sandwiched between the anolyte electrode and the central chamber for the selective shuttle of Cl^- anions, whereas a piece of Nafion 115 membrane was inserted between the catholyte electrode and the central chamber for the selective shuttle of Na^+ cations. All batteries were galvanostatically cycled at 5 mA/cm^2 between 0.0 and 1.2 V. To understand the impact of flow dynamic on desalination and energy storage performance, the operational flow rate was changed from 20 to 40 and 60 mL/min for all three channels, the MV anolyte, the $Na_4[Fe(CN)_6]$ catholyte, and the central brine solution. More experimental details for the battery configuration and testing conditions are included in the supporting information.

Once the flow rate was increased, the voltage gap between the charge and discharge curves that represents the cycling overpotential between charge and discharge steps was narrowed,

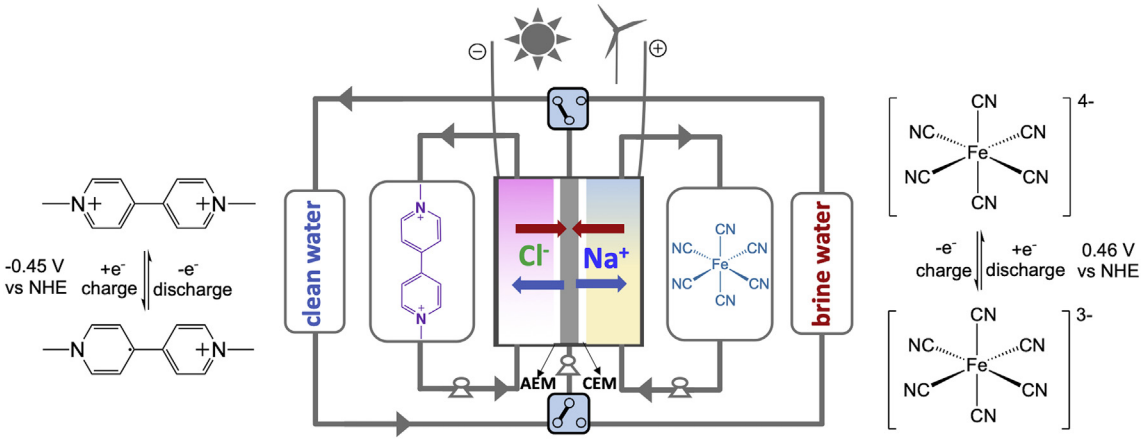

Fig. 1. A schematic illustration of the MV/$Na_4[Fe(CN)_6]$ desalination flow battery (DSRFB) and its cell reactions. Red and blue arrows illustrate the transport of sodium (Na^+) and chloride (Cl^-) ions during charge-salination and discharge-desalination processes.

indicating the battery became more conductive at a higher flow rate (Fig. 2A). Consequently, the battery capacity was increased along the flow rate, 137.04 mAh for 20 mL/min, 144.94 mAh for 40 mL/min, and 145.0 for 60 mL/min. The energy efficiencies of the DSRFB manifested are 56% for 20 mL/min, 64% for 40 mL/min, and 64% for 60 mL/min, respectively (Fig. 2B). The coulombic efficiency of the DSRFB was also improved from 94.8% to 96.2% from 20 to 60 mL/min. More importantly, the desalination percentage was apparently increased from 86.9% at 20 mL/min to 92.4% at 40 and 93.9% at 60 mL/min (Fig. 2B). As displayed in Fig. 2C and D, power performance of the DSRFB was evaluated using polarization studies under 50% and 100% state of charge (SOC) at three flow rates. Either at 50% or 100% SOC, increasing the flow rate has a positive impact on the battery power density, which is similar to what we observed in the battery capacity and efficiency studies. At 100% SOC, the determined peak power densities were gradually improved in the order of 14.72 mW/cm^2 at 20 mL/min, 15.15 mW/cm^2 at 40 mL/min, and 15.33 mW/mL at 60 mL/min. Even at 50% SOC, a peak power density of 10.5 mW/cm^2 was obtained at 60 mL/min. Furthermore, the response current densities for the observed peak power densities was also increased from 33.1 at 20 mL/min to 35.1 mA/cm^2 at 60 mL/min at 100% SOC.

2.2. Electrochemical impedance studies of the $MVCl_2/Na_4Fe(CN)_6$ desalination AORFB

To gain an in-depth understanding of the flow rate effect and monitor the status of the flow battery under different flow rates and SOCs, the 0.5 M MV/$Na_4[Fe(CN)_6]$ desalination AORFB was systematically examined by electrochemical impedance spectroscopy (EIS) studies (Fig. 3). Specifically, EIS tests were conducted at 0%, 50%, and 100% state of charge and discharge (SOC, SOD) at each flow rate to inspect the change of the battery ohmic resistance during the charge-salination and discharge-desalination processes. The EIS Nyquist plots are displayed in Fig. 3A–C for the charge-salination process and in Fig. 3D–F for the discharge-desalination process. As clearly depicted in Fig. 3, the ohmic resistance of the cell showed an inverse correlation with the flow rate. At 0% SOC, the ohmic resistance has shown a large decrease from 17.01 Ω*cm^2 at 20 mL/min (blue curve in Fig. 3A) to 12.89–1289 Ω*cm^2 at 40 mL/min (green curve in Fig. 3A), and further down to 11.60 Ω*cm^2 at 60 mL/min (orange curve in Fig. 3A). A similar trend was observed at 50% and 100% SOC (Fig. 3B and C). Interestingly, under 100% SOC, the reduction of the battery resistance improved by the flow rate change was less sensitive than 0% and 50% SOC (Fig. 3G). This could be attributed to the conductivity change at the central chamber. As the central chamber solution was concentrated at 100% SOC, the whole system became more conductive than those at 0% and 50% SOC at all three flow rates. For example, at 20 mL/min, an ohmic resistance of 14.88 Ω*cm^2 was observed at 100% SOC compared with 15.38 Ω*cm^2 at 50% SOC, and 17.01 Ω*cm^2 at 0% SOC (Fig. 3G). Thus, the effect of the flow rate was less significant at 100% SOC.

During the discharge-desalination process, a similar trend for the battery ohmic resistance was observed with the change of the flow rate at each state of discharge (SOD, Fig. 3D–F and H). At the beginning of the discharge-desalination process, the battery ohmic resistance was increased to 16.26 Ω*cm^2 (Fig. 3D, orange curve) from 14.88 Ω*cm^2 (Fig. 3C, orange curve) after the 100% SOC charge-salination process at 20 mL/min because of replacing the

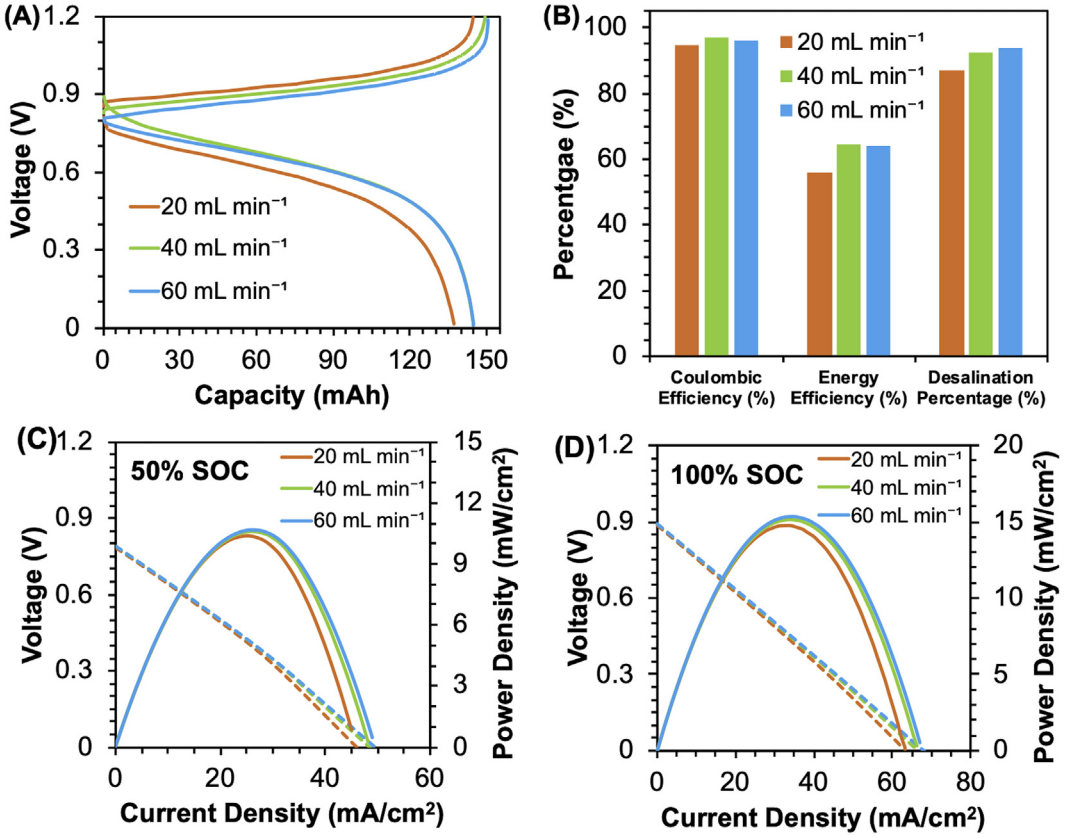

Fig. 2. (A) Charge and discharge curves of the 0.5 M MV/$Na_4[Fe(CN)_6]$ DSRFB under different flow rates at 5.0 mA/cm^2. (B) Coulombic efficiencies, energy efficiencies, and desalination percentages under different flow rates of the DSRFB. (C) Polarization and power density curves for the 50% SOC of the DSRFB under different flow rates. (D) Polarization and power density curves for the 100% SOC of the DSRFB under different flow rates.

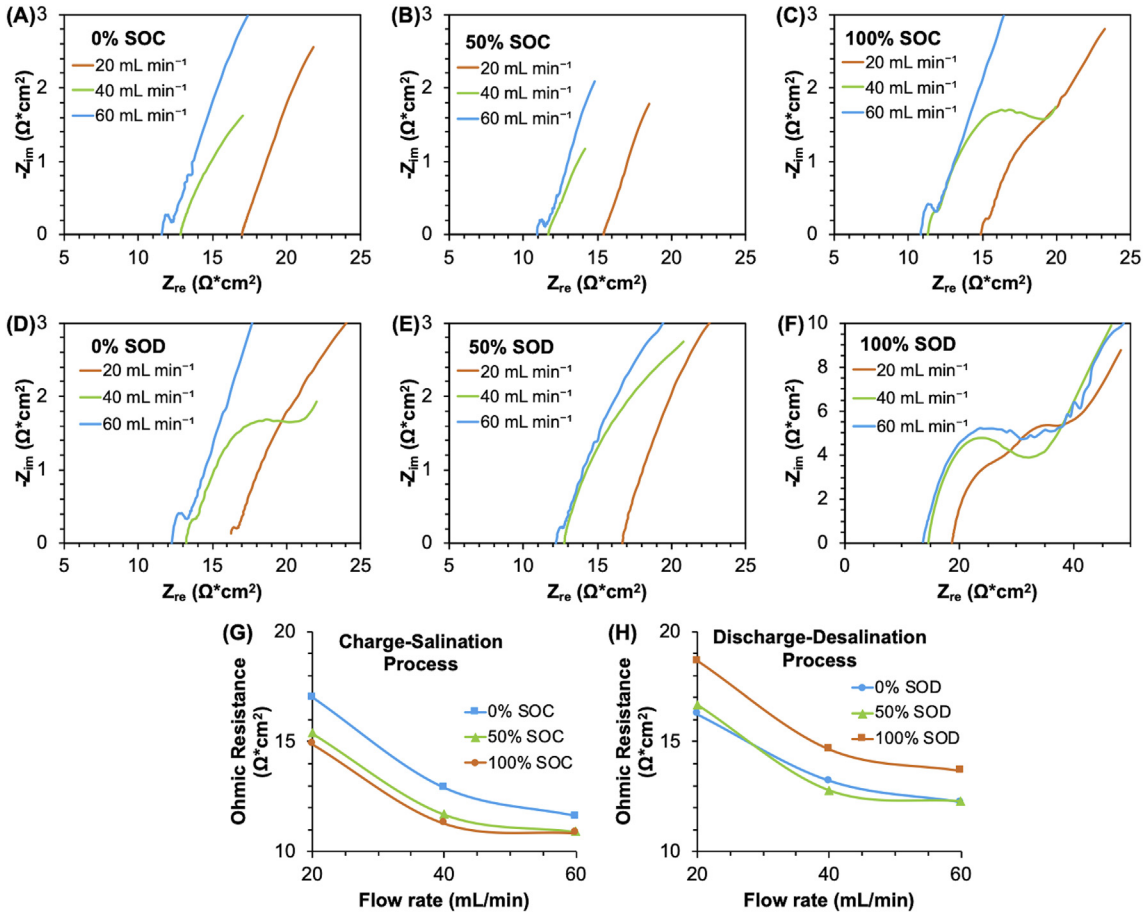

Fig. 3. EIS Nyquist plots of the 0.5 M MV/$Na_4[Fe(CN)_6]$ DSRFB collected at 0% SOC (A), 50% SOC (B), and 100% SOC (C) during the charge-salination process and at 0% SOD (D), 50% SOD (E), and 100% SOD (F) during the discharge-desalination process under the flow rates of 20, 40, and 60 mL/min. (G) Ohmic resistance change of the DSRFB during charge-salination process. (H) Ohmic resistance change of the DSRFB during discharge-desalination process.

solution in the central channel. With the increase of the flow rate from 20 to 60 mL/min, the battery ohmic resistance decreased from 16.26 to 12.24 Ω*cm^2 (Fig. 3D). Because the central channel solution undergoes desalination during the discharge process, the ohmic resistance through this process kept increasing under each flow rate. For example, at 20 mL/min, the battery ohmic resistance was increased from 16.26 Ω*cm^2 at 0% SOD to 16.65 Ω*cm^2 at 50% SOD and 18.66 Ω*cm^2 at 100% SOD. At 60 mL/min, the battery ohmic resistance at 0% SOC (the end of the discharge-desalination process) was lowered to 13.68 Ω*cm^2. It is believed that the charge transfer resistance and mass transport resistance are also benefitted from the increase of flow rates. However, the semicircles expressing the charge transfer resistances are not clearly resolved in all EIS studies. Still at 0% SOD (Fig. 3D), the charge transfer resistance was observed to decrease from 1.5 Ω*cm^2 at 20 mL/min to 1.0 Ω*cm^2 at 40 mL/min, and 0.5 Ω*cm^2 at 60 mL/min. Overall, it can be explained that the reduced battery resistance by increasing the flow rate leads to the improved energy efficiencies, desalination efficiencies, and power densities discussed above (Fig. 2).

3. Conclusion

In summary, we have established a relationship between the flow rate and energy storage and desalination performance of the MV/$Na_4Fe(CN)_6$ DSRFB. We found that the increase of flow rate facilitates the mass transfer process and reduces the battery ohmic and charge transfer resistances. Specifically, by increasing the flow rate from 20 to 60 mL/min, the desalination flow batteries demonstrated performance improvement for energy efficiency, desalination percentage, and power performance respectively. These new findings open a new engineering direction for the optimization of desalination flow batteries.

Declaration of competing interest

The authors declare that they have no known competing financial interests or personal relationships that could have appeared to influence the work reported in this article.

Acknowledgments

The authors thank Utah State University for providing faculty startup funds to the PI (T. Leo Liu) for supporting this study. We acknowledge National Science Foundation Career Award (Grant No. 1847674) for supporting a portion of research assistantship for W.W.

Appendix A. Supplementary data

Supplementary data to this article can be found online at https://doi.org/10.1016/j.mtener.2021.100750.

References

[1] R.F. Service, Desalination freshens up, Science 313 (5790) (2006) 1088–1090.
[2] M. Elimelech, W.A. Phillip, The future of seawater desalination: energy, technology, and the environment, Science 333 (6043) (2011) 712–717.
[3] M.A. Shannon, P.W. Bohn, M. Elimelech, J.G. Georgiadis, B.J. Mariñas, A.M. Mayes, Science and technology for water purification in the coming decades, Nature 452 (2008) 301.
[4] A.D. Khawaji, I.K. Kutubkhanah, J.-M. Wie, Advances in seawater desalination technologies, Desalination 221 (1) (2008) 47–69.
[5] M.E. Suss, V. Presser, Water desalination with energy storage electrode materials, Joule 2 (1) (2018) 10–15.
[6] J. Luo, B. Hu, M. Hu, Y. Zhao, T.L. Liu, Status and prospects of organic redox flow batteries towards sustainable energy storage, ACS Energy Lett. 4 (2019) 2220–2236.
[7] X. Wei, W. Pan, W. Duan, A. Hollas, Z. Yang, B. Li, Z. Nie, J. Liu, D. Reed, W. Wang, V. Sprenkle, Materials and systems for organic redox flow batteries: status and challenges, ACS Energy Lett. 2 (2017) 2187–2204.
[8] Y. Ding, C. Zhang, L. Zhang, Y. Zhou, G. Yu, Molecular engineering of organic electroactive materials for redox flow batteries, Chem. Soc. Rev. 47 (2017) 69–103.
[9] J. Winsberg, T. Hagemann, T. Janoschka, M.D. Hager, U.S. Schubert, Redox-flow batteries: from metals to organic redox-active materials, Angew. Chem. Int. Ed. 56 (2016) 686–711.
[10] T. Liu, X. Wei, Z. Nie, V. Sprenkle, W. Wang, A total organic aqueous redox flow battery employing a low cost and sustainable methyl viologen anolyte and 4-HO-TEMPO catholyte, Adv. Energy Mater. 6 (3) (2016) 1501449.
[11] B. Hu, C. DeBruler, Z. Rhodes, T.L. Liu, Long-cycling aqueous organic redox flow battery (AORFB) toward sustainable and safe energy storage, J. Am. Chem. Soc. 139 (3) (2017) 1207–1214.
[12] C. DeBruler, B. Hu, J. Moss, X. Liu, J. Luo, Y. Sun, T.L. Liu, Designer two-electron storage viologen anolyte materials for neutral aqueous organic redox flow batteries, Inside Chem. 3 (2017) 1–18.
[13] C. DeBruler, B. Hu, J. Moss, J. Luo, T.L. Liu, A sulfonate-functionalized viologen enabling neutral cation exchange, aqueous organic redox flow batteries toward renewable energy storage, ACS Energy Lett. 3 (2018) 663–668.
[14] T. Janoschka, N. Martin, M.D. Hager, U.S. Schubert, An aqueous redox-flow battery with high capacity and power: the TEMPTMA/MV system, Angew. Chem. Int. Ed. 55 (46) (2016) 14427–14430.
[15] J. Winsberg, T. Janoschka, S. Morgenstern, T. Hagemann, S. Muench, G. Hauffman, J.-F. Gohy, M.D. Hager, U.S. Schubert, Poly(TEMPO)/Zinc hybrid-flow battery: a novel, “green,” high voltage, and safe energy storage system, Adv. Mater. 28 (11) (2016) 2238–2243.
[16] E.S. Beh, D. De Porcellinis, R.L. Gracia, K.T. Xia, R.G. Gordon, M.J. Aziz, A neutral pH aqueous organic–organometallic redox flow battery with extremely high capacity retention, ACS Energy Lett. 2 (2017) 639–644.
[17] J. Luo, B. Hu, C. Debruler, T.L. Liu, A π-conjugation extended viologen as a two-electron storage anolyte for total organic aqueous redox flow batteries, Angew. Chem. Int. Ed. 57 (2018) 231–235.
[18] Y. Liu, M.-A. Goulet, L. Tong, Y. Liu, Y. Ji, L. Wu, R.G. Gordon, M.J. Aziz, Z. Yang, T. Xu, A long-lifetime all-organic aqueous flow battery utilizing TMAP-TEMPO radical, Inside Chem. 5 (7) (2019) 1861–1870.
[19] B. Huskinson, M.P. Marshak, C. Suh, S. Er, M.R. Gerhardt, C.J. Galvin, X. Chen, A. Aspuru-Guzik, R.G. Gordon, M.J. Aziz, A metal-free organic-inorganic aqueous flow battery, Nature 505 (7482) (2014) 195–198.
[20] B. Yang, L. Hoober-Burkhardt, F. Wang, G.K. Surya Prakash, S.R. Narayanan, An inexpensive aqueous flow battery for large-scale electrical energy storage based on water-soluble organic redox couples, J. Electrochem. Soc. 161 (9) (2014) A1371–A1380.
[21] A. Hollas, X. Wei, V. Murugesan, Z. Nie, B. Li, D. Reed, J. Liu, V. Sprenkle, W. Wang, A biomimetic high-capacity phenazine-based anolyte for aqueous organic redox flow batteries, Nat. Energy 3 (6) (2018) 508–514.
[22] J. Luo, B. Hu, C. Debruler, Y. Bi, Y. Zhao, B. Yuan, M. Hu, W. Wu, T.L. Liu, Unprecedented capacity and stability of ammonium ferrocyanide catholyte in pH neutral aqueous redox flow batteries, Joule 3 (2019) 1–15.
[23] J. Luo, A. Sam, B. Hu, C. DeBruler, X. Wei, W. Wang, T.L. Liu, Unraveling pH dependent cycling stability of ferricyanide/ferrocyanide in redox flow batteries, Nanomater. Energy 42 (2017) 215–221.
[24] Y. Chen, M. Zhou, Y. Xia, X. Wang, Y. Liu, Y. Yao, H. Zhang, Y. Li, S. Lu, W. Qin, X. Wu, Q. Wang, A stable and high-capacity redox targeting-based electrolyte for aqueous flow batteries, Joule 3 (9) (2019) 2255–2267.
[25] C. Zhang, Z. Niu, S. Peng, Y. Ding, L. Zhang, X. Guo, Y. Zhao, G. Yu, Phenothiazine-Based organic catholyte for high-capacity and long-life aqueous redox flow batteries, Adv. Mater. 31 (24) (2019) 1901052.
[26] W. Liu, Z. Zhao, T. Li, S. Li, H. Zhang, X. Li, A high potential biphenol derivative cathode: toward a highly stable air-insensitive aqueous organic flow battery, Sci. Bull. 66 (5) (2021) 457–463.
[27] D. Desai, E.S. Beh, S. Sahu, V. Vedharathinam, Q. van Overmeere, C.F. de Lannoy, A.P. Jose, A.R. Völkel, J.B. Rivest, Electrochemical desalination of seawater and hypersaline brines with coupled electricity storage, ACS Energy Lett. 3 (2) (2018) 375–379.
[28] X. Hou, Q. Liang, X. Hu, Y. Zhou, Q. Ru, F. Chen, S. Hu, Coupling desalination and energy storage with redox flow electrodes, Nanoscale 10 (2018) 12308–12314.
[29] Q. Liang, F. Chen, S. Wang, Q. Ru, Q. He, X. Hou, C.-y. Su, Y. Shi, An organic flow desalination battery, Energy Storage Mater. 20 (2019) 203–207.
[30] C. Debruler, W. Wu, K. Cox, B. Vanness, T.L. Liu, Integrated saltwater desalination and energy storage through a pH neutral aqueous organic redox flow battery, Adv. Funct. Mater. 30 (2020) 2000385.
[31] F. Chen, J. Wang, Q. Ru, S.H. Aung, T.Z. Oo, B. Chu, Continuous electrochemical desalination via a viologen redox flow reaction, J. Electrochem. Soc. 167 (8) (2020), 083503.